Modeling of Circulating Fluidized Beds Systems for Post-Combustion CO_2 Capture via Temperature Swing Adsorption

Stefano E. Zanco and Marco Mazzotti
ETH Zurich, Institute of Process Engineering, Sonneggstrasse 3, Zurich 8092, Switzerland

Matteo Gazzani
Copernicus Institute of Sustainable Development, Utrecht University, Heidelberglaan 2, Utrecht, CS 3584, The Netherlands

Matteo C. Romano and Isabel Martínez
Dept. of Energy, Politecnico di Milano, via Lambruschini 4, Milano 20156, Italy

DOI 10.1002/aic.16029
Published online December 6, 2017 in Wiley Online Library (wileyonlinelibrary.com)

The technology of circulating fluidized beds (CFBs) is applied to temperature swing adsorption (TSA) processes for post-combustion CO_2 capture employing a commercial zeolite sorbent. Steady state operation is simulated through a one-dimensional model, which combines binary adsorption with the CFB dynamics. Both single step and multi-step arrangements are investigated. Extensive sensitivity analyses are performed varying the operating conditions, in order to assess the influence of the main operational parameters. The results reveal a neat superiority of multi-step configurations over the standard one, in terms of both separation performance and efficiency. Compared to fixed-bed TSA systems, CFB TSA features a high compactness degree. However, product purity levels are limited compared to the best performing fixed-bed processes, and heat management within the system appears to be a major issue. As regards energy efficiency, CFB systems place themselves in between the most established absorption-based technologies and the fixed-bed TSA. © 2017 The Authors AIChE Journal published by Wiley Periodicals, Inc. on behalf of American Institute of Chemical Engineers *AIChE J*, 64: 1744–1759, 2018

Keywords: temperature swing adsorption, circulating fluidized bed, post-combustion carbon capture, CCS

Introduction

A wide variety of different methods have been proposed in literature to capture CO_2 from large stationary point sources, especially power plants.[1] Nowadays the most established technology is represented by post-combustion systems based on absorption processes, where aqueous solutions of amines are employed to separate CO_2 from the flue gas mixture. Following several pilot and demonstration projects,[2–5] this technology can be regarded as commercial and ready for massive deployment. However, because of (1) the impact of the regeneration step on the overall energy balance of the plant and (2) the complexity in managing liquid solvents in power plants (e.g., amine degradation, aerosol formation), the research for second generation technologies is undoubtedly a topic of great current interest.[6]

In particular, the possibility of following an adsorption-based route has been recently contemplated. The regeneration of solid sorbents, compared to liquid ones, requires on average a smaller amount of energy. Moreover, solids are not volatile and commonly do not pose any health hazard. At the same time, solid sorbents allow achieving similar or even superior separation performance, compared to absorption-based processes. For these reasons adsorption-based technologies appear to be promising alternatives for the same post- and pre-combustion applications where the suitability of the absorption processes has already been proven.[7,8]

When solid sorbents are employed in a large scale separation process, the regeneration step is commonly performed by means of either pressure swing adsorption (PSA) or temperature swing adsorption (TSA) cycles, in which the thermodynamic properties of the solids are manipulated by changing the pressure or temperature levels of the system, respectively. In addition, the two different routes can be combined when designing a cycle, so as to maximize the efficiency of the sorbent regeneration for given temperature and pressure ranges. PSA processes are commercially available for the purification of the light (i.e., less retained) component (e.g., hydrogen production from NG-based syngas), whereas TSA cycles have shown interesting performance for the recovery of the heavy component from ambient pressure streams (e.g., water removal from air in cryogenic air separation units and CO_2 removal from flue gas).[9–12] Indeed, in

Correspondence concerning this article should be addressed to M. Mazzotti at marco.mazzotti@ipe.mavt.ethz.ch.

the latter case there is no need to maintain the feed stream or the products at a pressure different from ambient conditions. This allows to avoid energy intensive compression of the flue gas or drawing vacuum in the vessels. Moreover, most solid sorbents can be conveniently regenerated at relatively low temperature, so that a low-grade heat source may be employed, possibly recovering waste heat from other plant units.

Promising results, in terms of both separation performance and overall efficiency, were reported in the work by Joss et al.,[13] where the design of new TSA cycles enabled the removal of CO_2 from flue gas by means of commercial sorbents (Zeolite 13X) and conventional vessel design (shell-and-tube heat exchangers) with energy needs and productivity close to those of absorption processes. However, it was shown that fixed bed TSA suffers from two main drawbacks: (1) The energy consumption must account for the heating and cooling of the bed, and (2) a large footprint is required to process large flow rates. Therefore, in this work we investigate the possibility of designing a TSA process in circulating fluidized bed (CFB) reactors, as an alternative to the most traditional fixed bed solutions.

Although fluidized beds represent an already established technology and are extensively employed in a wide variety of industrial processes since the beginning of the last century, combining adsorption with the fluidization of the sorbent bed is a recent proposal, which has not been thoroughly investigated yet. As regards the use of fluidized beds for the capture of CO_2 through adsorption at ambient temperature, a few studies have been published about the topic. This reactor technology has been both theoretically and experimentally assessed, producing results for different fluidization regimes and for a broad range of CO_2 concentrations, from atmospheric air conditions to flue gas.[14–17] Standard dual fluidized bed systems have been proposed as energy efficient alternatives to amine scrubbing, both in the form of low temperature carbonation cycles[18] or as continuous TSA applications.[19] Also more complex configurations have been proposed, where multi-stage systems are coupled with intra- and interstage heat recovery.[20–22] Most systems employ bubbling beds for both the adsorption and the regeneration section: this fluidization regime allows for effective heat transfer and for relatively high volumetric gas flow rates.

Thanks to their fast fluidization, CFBs possess key advantages over both fixed-bed systems and bubbling beds: (1) The higher gas velocity allows minimizing the plant size and footprint (and therefore the capital expenditure associated therewith), especially in application with large volumetric flow rates as in post-combustion CO_2 capture; (2) the fluidization regime typical of CFBs is very effective in promoting heat exchange both between gas and solid phase and between suspension and riser walls, which enables precise control of the temperature within the bed and reduced heat transfer surface to provide and remove the process heat; (3) CFBs can operate continuously as steady state reactors that undergo adsorption and regeneration, thus reducing the number of units and the amount of energy needed for the temperature swing, completely relying on entrainment as a mechanism for the displacement of the solids.

All these studies suggest that such processes could be a potentially cost-effective and promising alternative for the handling of power plant flue gas. Nevertheless, previous results obtained by Pirngruber et al.[23] have highlighted serious complications in performing TSA cycles inside fluidized beds, mostly due to unfavorable limitations occurring in the regeneration phase. Moreover, even when specifically designed solid sorbents have been used, fluidized bed systems do not outperform the absorption processes.

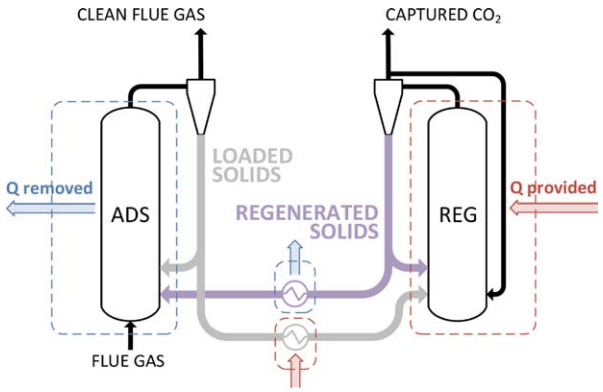

Figure 1. Single step configuration layout.

[Color figure can be viewed at wileyonlinelibrary.com.]

With this contribution we aim at developing a model for a dual fast-fluidized bed adsorption system, which stands for a first principle description of such system with a new dedicated simulation approach. Moreover, advanced adsorber configurations are proposed and assessed for adsorption-based CO_2 capture processes, evaluating their performance as a function of a set of operating parameters. Finally, the performance of the simulated systems is compared with that of the benchmark amine scrubbing techniques.

TSA Processes for CO_2 Capture in CFBs

Standard plant configuration: Single step

The simplest CFB system for CO_2 separation via adsorption consists of two separated CFB reactors, one for the adsorption stage and one for the regeneration phase. Figure 1 illustrates the layout of this basic system configuration.

The adsorber is fluidized by the flue gas, which is fed at its bottom after being dried. At the same time, regenerated solids enter the vessel. The heat released by adsorption as well as the sensible heat released by the regenerated solids are removed by exchange with the external cooling system. Adsorption proceeds along the bed, CO_2 is transferred from the gas phase to the solid particles. At the outlet, the decarbonized flue gas entrains the loaded solids into a cyclone separator, where solids are collected. A fraction of the solids collected in the cyclone is recirculated to the reactor, whereas the rest is sent to the regeneration unit. The CO_2-lean gas is sent to the stack or to a downstream process unit.

In the regenerator, the loaded solids release the adsorbed molecules due to the higher temperature. The heat required to heat up the solids and to keep the temperature constant while the endothermic desorption occurs is provided by an external heating system. The regenerated solids that exit the reactor are retrieved by means of a cyclone separator and recirculated to the regenerator inlet or conveyed back to the adsorption unit. Steam is usually employed as stripping gas in the desorber,[21] as it can be easily separated from the recovered CO_2 in a downstream unit. In presence of a water-adsorbing sorbent, like the zeolitic material adopted here, a dry stripping gas must be used. For this reason, in our configuration the gas stream consisting of recovered CO_2 is partially recycled to fluidize the bed, similarly to what is proposed by Kim et al.,[20] whereas the rest of the gas is sent to compression for further storage.

The size of the adsorber, in terms of height and cross section, is adapted according to the flow rate of flue gas that is

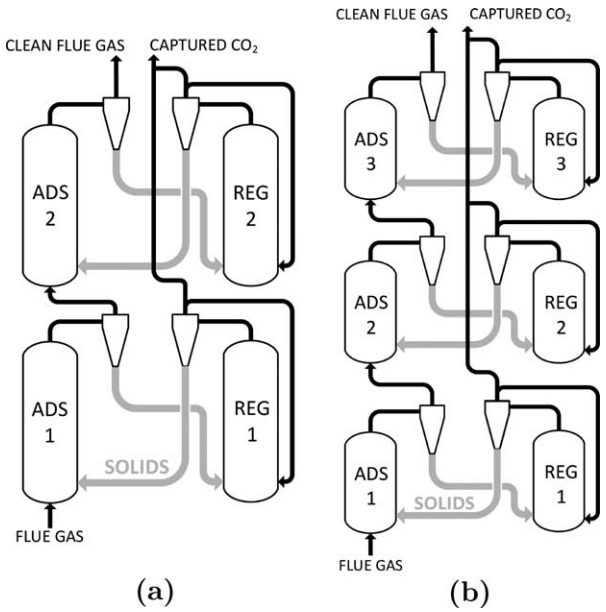

Figure 2. (a) Two-step and (b) three-step isolated multi-step configurations.

For the sake of simplicity, solids recirculation loops, and heat exchangers are not shown.

processed. As regards the regenerator, the same height and cross section are adopted, while the inlet flow rate of recirculated gas is adjusted according to the gas properties, in order to maintain the same superficial velocity at the inlet of both vessels.

Alternative plant configurations: Isolated multistep configurations

While, on the one hand, the high mixing rate of the sorbent within the fluidized bed enhances heat exchange, on the other hand, it does not allow to selectively convey the less loaded solids to where the CO_2 gas phase concentration is lower, which would further promote the removal of CO_2 from the flue gas. Therefore, in order to increase the performance over the limits reached by the standard configuration, alternative plant configurations must be adopted.

Dividing each reactor into different stages allows to overcome this limitation. In fact, by arranging different adsorption steps in series, different average solid loadings will be established within each adsorber. The least loaded solids can be thus employed where the gas phase concentration is lower so as to recover higher amounts of CO_2.

In the regeneration section, where the gas phase concentration is almost constant along the vessel due to the gas recirculation, a division into stages would benefit the CO_2 desorption only to a lower extent.

In the first novel configuration presented in this work, each adsorber is coupled to a dedicated regenerator (see Figure 2). Multiple consecutive adsorption-regeneration blocks are present, each of them looping its own solid inventory and operating with a specific sorbent cyclic capacity, which in principle depends on the gas phase concentration in the adsorber. The blocks form a so-called multi-step "isolated" configuration, thus expressing the fact that each step consists in an independent adsorption-regeneration loop. In fact, the only connection between a block and the previous or the following one is the treated flue gas, which flows directly from the outlet of an adsorption unit to the inlet of the following one.

Also the composition of the gas stream recirculated to fluidize the regenerator is different from block to block, which corresponds to a series of product streams (one for each desorber) with different specifications. For a decreasing CO_2 concentration in the adsorber (i.e., proceeding from bottom to top in Figure 2), the ratio between adsorbed CO_2 and adsorbed N_2 at adsorber outlet decreases and this is conducive to a higher N_2 concentration in the regenerator, which corresponds to a lower product purity, but also to a better regenerated sorbent (i.e., leaving the regenerator with a lower adsorbed amount of CO_2).

The number of adsorption and desorption steps depends on the trade-off between the enhancement of the performance and the increase in system complexity. Some sensitivity analyses, which have been conducted varying the number of blocks, have shown that the relative improvement in separation performance connected to the addition of a step decreases with the total number of steps. After the third block, any benefit deriving from a further addition is likely to be too small to justify the adoption of a more complex configuration. For this reason, two-step and three-step configurations are considered here.

In order to make a consistent comparison with the single step configuration, for multiple step configurations the same cross section and total height of the adsorption and regeneration sections are used. This implies that, for a fixed inventory, the same total amount of solids is distributed into a different number of adsorbers depending on the number of blocks.

Alternative plant configurations: Counter-current multistep

As mentioned above, introducing a division into stages for the regeneration section, where the gas phase concentrations are almost constant along the vessel, does not enhance the separation performance significantly. At the same time, adopting an "isolated" configuration, might compromise the final purity of the recovered CO_2, because in the last steps a significant amount of nitrogen is adsorbed in the adsorption section, due to high N_2 concentrations.

Therefore, in this second approach, only the adsorption stage is divided into multiple vessels, through which both gas and solids flow sequentially. As the definition "counter-current" suggests, the path followed by the solid sorbent through the adsorption units is opposite to that followed by the gas. The first vessel the gas passes through (i.e., ADS 1) is the last entered by the solids after regeneration, similarly to what have been proposed by Pröll et al.[21] In analogy with the standard configuration, the regeneration section consists of a single vessel.

In such configuration, the least loaded sorbent particles (those exiting the regenerator) are contacted at first with the flue gas where the CO_2 content is the lowest, i.e., at the end of the adsorption section. In such a way the mass transfer driving force is enhanced by the low sorbent loading and the separation proceeds further, despite the low CO_2 concentration. In this instance, the high gas phase concentration of N_2 causes a significant amount of nitrogen to adsorb as well. The solids are later conveyed to the other adsorbers, where the CO_2 gas phase concentration is higher and, due to the competitive adsorption behavior of the two species, the concentration of CO_2 in the adsorbed phase increases, partly also at the expenses of that of N_2.

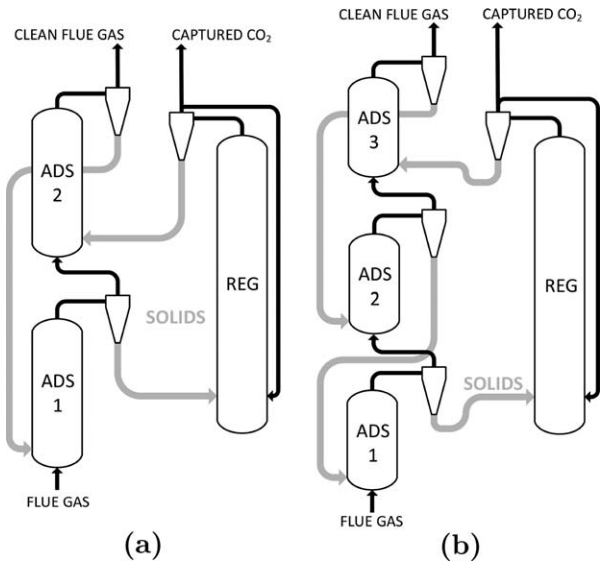

Figure 3. (a) Two-step and (b) three-step counter-current multistep configurations.

For the sake of simplicity, solids recirculation loops, and heat exchangers are not shown.

The adsorption stage might be divided into any number of adsorbers. Consistently with what is done for the cocurrent configurations, two-step and three-step systems are simulated. In order for them to be compared, the total vessel volume of the whole adsorption side is kept constant and divided into two or three reactors, depending on the configuration; the cross section is the same for all adsorbers, whereas the total height is equally divided among the steps, as schematically shown in Figure 3. As regards the regeneration section, the reactor is analogous to that of the single step configuration.

Adsorption Processes in CFB Reactors

Modeling approach

Assumptions. In this work, the CFBs used for sorption and regeneration are described by a steady state one-dimensional model (with the axial coordinate being the only independent variable). The following assumptions are made:

1. Solids inside the riser are assumed to be perfectly mixed (i.e., as in a continuous stirred-tank reactor, CSTR) with regards to temperature and adsorbate loading. This hypothesis is acceptable for fast fluidization regimes, like those of CFBs, where high velocities and low solid volumetric fractions enhance particle mixing to a great extent. Moreover, the solid inventory is only partially conveyed out of the reactor, because along the reactor many particles slow down and fall back, thus resulting in a strong internal recirculation.

2. Gases flow along the bed like a plug flow: The composition progressively changes along the riser length, as well as its velocity, as adsorption proceeds.

3. Thermal equilibrium is immediately established between gas and solid phase. The fast mixing of solids in CFBs is conducive to high heat transfer coefficients between gas and solids, which prevent the onset of significant temperature gradients within and between the two phases. Consistently, and given the stationary operation of the system, it is assumed that each reactor operates isothermally at an assigned temperature. The energy balance over the riser is satisfied by exchanging heat with an external fluid through the surface available at the reactor walls.

4. Pressure is constant throughout the bed, i.e., pressure drop is negligible along the riser.

5. Gases are described as ideal gas mixtures.

6. Neither chemical reactions nor sorbent deactivation occur.

As a consequence of the hypotheses above, mass and momentum balances can be decoupled from the energy balance, because of the isothermal operation. Moreover, no explicit expression for the momentum balance is needed, since the pressure is uniform along the reactor.

Mass Balance. As regards the mass balance, the operation of the system can be simulated by coupling two models. On the one hand, the CSTR model for the solid phase, which corresponds to N component mass balances over the whole vessel, according to assumption 1:

$$u^{\text{inlet}}\, C_i^{\text{inlet}} - u^{\text{outlet}}\, C_i^{\text{outlet}} = G_{\text{R}} \left(\bar{n}_i - n_i^{\text{inlet}}\right) \;\; \forall\, i = 1, \cdots, N \tag{1}$$

where G_{R} is the mass flow rate of fresh sorbent fed at bed inlet, specific per cross section surface unit; n_i^{inlet} is the amount of adsorbed phase carried by the solid entering the riser (the loading of the regenerated sorbents, which would be zero in case of a full regeneration); $\bar{n}_i$ is the particle loading within the reactor, equal to the loading at the outlet; C_i is the gas phase concentration of the i-th species; u is the superficial velocity of the gas.

On the other hand, the plug flow model used for the gas phase consists of $N + 1$ mass balance equations, one for each component plus the overall balance:

$$\begin{cases} \dfrac{\mathrm{d}(u\, C_i)}{\mathrm{d}z} + \rho_{\text{s}}\, \varepsilon_{\text{s}}(z)\, \bar{r}_i(\underline{C}) = 0 & \forall\, i = 1, \cdots, N \\ \dfrac{\mathrm{d}(u\, C_{\text{mix}})}{\mathrm{d}z} + \rho_{\text{s}}\, \varepsilon_{\text{s}}(z) \displaystyle\sum_{i=1}^{N} \bar{r}_i(\underline{C}) = 0 \end{cases} \tag{2}$$

being ε_{s} the volumetric fraction of bed occupied by solids, which is a function of the axial coordinate z, according to the solid distribution within the riser; $\bar{r}_i$ is the adsorption rate for an average particle loading $\bar{n}_i$. The overall gas phase concentration C_{mix} is by definition equal to the sum of the concentrations of the single components and is a function of p and T only through the equation of state for ideal gases:

$$C_{\text{mix}} = \sum_{i=1}^{N} C_i = \frac{p}{RT} \tag{3}$$

It is constant throughout the reactor, because T and p do not depend on z according to the model assumptions.

Equilibria and Kinetics. In this study, adsorption isotherms are described by means of the Sips equation (Eq. 4), which has largely been used for binary, ternary, and other multi-component mixtures.[24,25] According to the model, for a mixture of N species considered as ideal gases, the amount of i-th component adsorbed per unit sorbent mass at equilibrium conditions, n_i^{eq}, is computed as:

$$n_i^{\text{eq}} = \frac{n_i^{\infty} \left(\kappa_i\, y_i\, p\right)^{\gamma_i}}{1 + \sum_{j=1}^{N} \left(\kappa_j\, y_j\, p\right)^{\gamma_j}} \forall\, i = 1, \cdots, N \tag{4}$$

where n_i^{∞} is the saturation capacity of the solid, κ_i is the equilibrium constant, and γ_i accounts for the inhomogeneity of the sorbent surface. All three parameters are temperature

dependent. The relation between the partial pressure of each component, $y_i p$, and the molar concentrations in Eqs. 2 and 3 is determined by the equation of state for ideal gases.

The amount of gas that is adsorbed in the solid under operating conditions of the reactor is established by the overall mass transfer resistance between the bulk gas phase and the available sites on the solid. Despite several mass transfer models exist, which account for the adsorption of a molecule from the bulk gas to the solid with different levels of detail, most approaches for separation processes make use of a linear driving force (LDF) model.[24] In this case the rate of adsorption is computed, considering an average sorbent particle loading $\bar{n}_i$, as

$$\bar{r}_i = \omega_i \left(n_i^{\mathrm{eq}}(\underline{C}) - \bar{n}_i \right) \tag{5}$$

where ω_i is the single lumped mass transfer parameter for the LDF model, assumed constant for each i-th gas species.

Solid Distribution Within the Riser. The solids inside the vessel are assumed to be distributed differently into two zones, namely a bottom dense region and an upper lean region, as suggested by Kunii and Levenspiel.[26] The distribution is described by the solid volumetric fraction, ε_s, which is constant in the dense region, whereas it decreases exponentially to an asymptotic value, $\varepsilon_s^{\mathrm{asym}}$, in the lean zone, according to the following expression:

$$\varepsilon_s(z) = \begin{cases} \varepsilon_s^{\mathrm{d}} & \text{for } z \in [0, H_{\mathrm{d}}] \\ \varepsilon_s^{\mathrm{asym}} + \left(\varepsilon_s^{\mathrm{d}} - \varepsilon_s^{\mathrm{asym}} \right) \exp\left(-\Lambda (z - H_{\mathrm{d}}) \right) & \text{for } z \in (H_{\mathrm{d}}, H_{\mathrm{t}}] \end{cases} \tag{6}$$

where the decay constant Λ is inversely proportional to the superficial velocity of the gas at the inlet, u^{inlet}. For a fixed fluidization regime and a chosen particle size, the value of the product $\Lambda u^{\mathrm{inlet}}$ is constant and can be inferred from experimental data reported in the literature.[26] The bottom dense zone height H_{d} is computed by imposing the condition that the amount of solids is equal to the given inventory, W_{s} (defined as mass of solids per unit cross section of the bed), i.e., from the following integral where H_{d} is the only unknown:

$$W_{\mathrm{s}} = \rho_{\mathrm{s}} \left[\varepsilon_{\mathrm{s}}^{\mathrm{d}} H_{\mathrm{d}} + \int_{H_{\mathrm{d}}}^{H_{\mathrm{t}}} \left(\varepsilon_{\mathrm{s}}^{\mathrm{asym}} + \left(\varepsilon_{\mathrm{s}}^{\mathrm{d}} - \varepsilon_{\mathrm{s}}^{\mathrm{asym}} \right) \exp\left(-\Lambda (z - H_{\mathrm{d}}) \right) \right) \mathrm{d}z \right] \tag{7}$$

Once the height of the bottom dense zone is known, the solid volumetric fraction at the riser outlet is:

$$\varepsilon_{\mathrm{s}}^{\mathrm{outlet}} = \varepsilon_{\mathrm{s}}^{\mathrm{asym}} + \left(\varepsilon_{\mathrm{s}}^{\mathrm{d}} - \varepsilon_{\mathrm{s}}^{\mathrm{asym}} \right) \exp\left(-\Lambda (H_{\mathrm{t}} - H_{\mathrm{d}}) \right) \tag{8}$$

hence the mass flow rate of entrained solids leaving the reactor per unit cross sectional area, G_{s}, is given by:

$$G_{\mathrm{s}} = \rho_{\mathrm{s}} \, \varepsilon_{\mathrm{s}}^{\mathrm{outlet}} \left(u^{\mathrm{outlet}} - u_{\mathrm{t}} \right) \tag{9}$$

where the terminal velocity of the solid particles, u_{t}, is estimated according to Heider and Levenspiel,[27] while the gas superficial velocity at the outlet, u^{outlet}, is calculated from the mass balance. Since the flow rate of solids recirculated between the reactors, G_{R}, which is a fixed input data of the model, is in general lower than G_{s}, a fraction R_{rec} of the entrained solids is recirculated back into the riser through a standpipe and a loop seal, while only the remaining fraction $(1 - R_{\mathrm{rec}})$ is sent to the following vessel. In this way, the same flow rate of solids enters and leaves the fluidized bed and the inventory of solids is maintained constant within it. The following relationship holds true:

$$G_{\mathrm{s}} = G_{\mathrm{R}} + R_{\mathrm{rec}} \, G_s \tag{10}$$

At every position along the riser, the conditions for entrainment and fluidization have to be satisfied; this means that the superficial velocity of the gas must exceed, respectively, the terminal velocity, u_t, and the minimum fluidization velocity, u_{mf}, that can be derived from the Ergun equation for minimum fluidization conditions.[26]

Energy Balance. The bed is assumed to operate at constant temperature T. The heat to be supplied or removed from the system, i.e., gas and solid phases, to maintain it at a T can be written as:

$$\begin{aligned} \dot{Q} = A \, G_{\mathrm{R}} & \left(c_{\mathrm{s}} + \sum_{i=1}^{N} n_i^{\mathrm{inlet}} M_{\mathrm{m},i} \, c_i^{\mathrm{ads}} \right) \left(T_{\mathrm{s}}^{\mathrm{inlet}} - T \right) + \\ & + A \, \rho_{\mathrm{mix}}^{\mathrm{inlet}} \, u^{\mathrm{inlet}} \, c_{\mathrm{p,mix}}^{\mathrm{inlet}} \left(T^{\mathrm{inlet}} - T \right) \\ & - A \, G_{\mathrm{R}} \sum_{i=1}^{N} \left(\left(n_i^{\mathrm{inlet}} - \bar{n}_i \right) \left(-\Delta h_i^{ads} \right) \right) \end{aligned} \tag{11}$$

where the first term on the right hand side accounts for the sensible heat of the solids, the second for the sensible heat of the gas and the third for the adsorption heat. The heat associated with the adsorption process, which would be conducive to a change in the temperature of the solids, is instantaneously transferred to the gas phase, according to the assumption of thermal equilibrium between the two phases.

The isothermal operation of the reactor at temperature T is enabled by exchanging such heat duty, $\dot{Q}$, through the reactor walls. Therefore, each reactor is coupled with a dedicated heat exchanger; the external side of the walls is in contact with a heat exchanging fluid flowing downwards in the axial direction at temperature T_{fluid}, which is in principle a function of the position. The heat transfer through the walls is modeled by means of the following energy balance for the system consisting of gas and solids:

$$\dot{Q} - \int_0^{H_{\mathrm{t}}} \left(\frac{1}{h_{\mathrm{susp}}(z)} + \frac{1}{h_{\mathrm{fluid}}(z)} \right)^{-1} \left(T - T_{\mathrm{fluid}}(z) \right) p_{\mathrm{exch}} \, \mathrm{d}z = 0 \tag{12}$$

where the differential heat exchanging surface in the infinitesimal length $\mathrm{d}z$ is given by the product $p_{\mathrm{exch}} \, \mathrm{d}z$, being p_{exch} the internal perimeter of the vessel cross section (i.e., the heat exchanger surface area per unit reactor height), which depends on the detailed design of the heat exchanger, something that is beyond the scope of this article. The internal and external surfaces of the walls are assumed to be equal and the conduction resistance of the steel wall is assumed to be negligible; only the convective heat transfer coefficients on the internal and external side of the walls, h_{susp} and h_{fluid}, respectively, are considered.

Heat Exchanger Geometry. In order to ensure a sufficiently large heat transfer surface inside the riser, each vessel is assumed to consist of a number of parallel compartments, separated by vertical heat transfer surfaces, as shown in Figure 4; from the point of view of the fluid dynamics of fluidization, each compartment operates as a separated riser. All these compartments have the same height, the same rectangular cross section with a fixed aspect ratio, θ, equal to 10 and the same specific (per cross section unit) inventory W_{s}. The heat transfer surfaces, i.e., the walls of the compartments, consist of single-

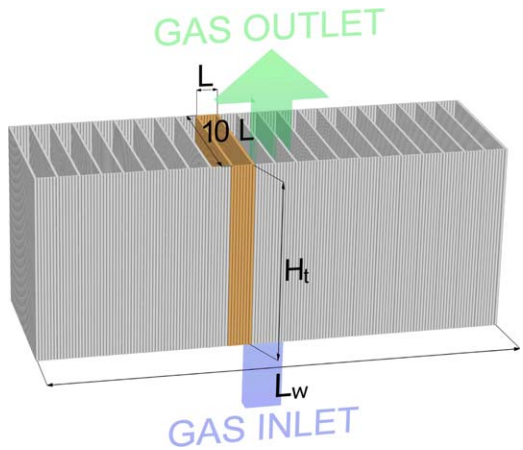

Figure 4. Schematic representation of the vessel geometry.

A single compartment is highlighted. The cross section aspect ratio of the single compartment, θ, is set to 10. The height of each compartment is equal to the height of the vessel, H_t. The total cross section of the vessel is given by a depth equal to θL and a width L_w. [Color figure can be viewed at wileyonlinelibrary.com.]

pass vertical steel tubes, so-called "walltubes," of diameter d_{WT}, wherein an external heat exchanging fluid flows.

The value of p_{exch} is determined by imposing that the energy balance at walls (Eq. 12) is satisfied; hence the length of short side of the short section, L, which represents the minimum distance between two parallel heat exchanging walls, is adjusted accordingly. For a given volumetric flow rate of gas and a given reactor height, the width of the vessel, L_w, can be computed once L is determined, as well as the depth, which is equal to the product θL.

Heat Transfer Coefficients. The first term to be assessed is the one related to the exchange between the solid–gas suspension and the riser walls, h_{susp}. However, determining the value of the suspension-to-wall coefficient inside a CFB is an open topic in literature.[26,28–30] Notably, not all available approaches are consistent with each other, as the available correlations are experimentally derived within a narrow range of operating conditions, that in many cases do not correspond to those investigated in this work. Nevertheless, the different studies agree upon the few following points: (1) radiation can be neglected when the temperature levels involved are sufficiently low, which is undoubtedly true for the application investigated here; (2) both conduction and convection should be taken into account, as the particles are believed to enhance the convective heat exchange due to gases discontinuously getting in direct contact with the walls; (3) this enhancement is in most correlations taken into account through a multiplying or an additional factor next to the gas-only convective coefficient, h_{go}, which is calculated assuming only gases are present inside the riser.

The following correlation proposed by Molodtsof and Muzyka[31] for gas-suspensions flowing inside ducts was originally developed for conditions relatively close to those of interest:

$$h_{susp} = h_{go} \frac{(1+M_r C_r)^2}{1+\alpha M_r C_r + \beta (M_r C_r)^2} \tag{13}$$

where M_r is the solid-to-gas loading ratio, derived from the density of the solids, ρ_s, and the density of the gas phase, ρ_{mix}, as

$$M_r = \frac{\varepsilon_s \rho_s}{(1-\varepsilon_s)\rho_{mix}} \tag{14}$$

and C_r is the solid-to-gas heat capacity ratio, i.e.,

$$C_r = \frac{c_s}{c_{p,mix}} \tag{15}$$

being c_s and $c_{p,mix}$ the specific heat capacities of the solids and the gas phase, respectively, while α and β are two parameters whose value is determined based on the fluid dynamic characteristics of the flow. A modification of the correlation, as proposed by Zhang et al.,[30] linearizes the previous expression, in such a way that it can be extended for a wider range of experimental data, including some conditions compatible with those investigated here:

$$h_{susp} = h_{go}(1+\gamma_h M_r C_r) \tag{16}$$

In this expression there is a single adjustable parameter γ_h, whereas h_{go} is estimated by means of the Gnielinski correlation.[32]

For cooling purposes water is used as external fluid. The temperature of water in the tubes, T_w is determined along the axial coordinate by a local energy balance at the wall as follows:

$$A_{WT} u_w \rho_w c_w \frac{dT_w}{dz} + \left(\frac{1}{h_{susp}(z)} + \frac{1}{h_w}\right)^{-1} (T_w - T) p_{exch} = 0 \tag{17}$$

where A_{WT} is the cumulative cross sections of all walltubes. Here the temperature dependent thermodynamic properties are kept constant, because their change is negligible in the relevant range of variation. The value of the convective heat transfer coefficient for water, h_w, is computed by means of the Dittus-Boelter correlation[29] from the properties of water at inlet temperature (density, ρ_w, specific heat capacity, c_w, and the other thermodynamic properties), which are considered constant, due to the reduced temperature variation along the heat exchanger.

For heating purposes, instead, condensing steam is used: the pressure of the steam is adjusted (up to the water critical point) in order to provide at the inlet a flow of saturated steam at a temperature higher than the fixed vessel temperature. The steam flows downwards in the tubes, so as to prevent any risk of flooding inside the pipes. The convective transfer coefficient of an annular flow of condensing steam can be computed by means of a correlation by Dobson and Chato,[33] which gives the value as a function of the vapor quality, x_v and of the velocity of the fluid. The profile of vapor quality along the axial coordinate is computed by means of a local energy balance at the wall:

$$A_{WT} u_v^{inlet} \rho_v^{inlet} \frac{dx_v}{dz} \Delta h_{lv}(T_v) + \left(\frac{1}{h_{susp}(z)} + \frac{1}{h_v(x_v, u_v, T_v)}\right)^{-1} (T_v - T) p_{exch} = 0 \tag{18}$$

The used properties of steam (density, ρ_v, and condensation enthalpy, Δh_{lv}) at different temperature and pressure levels are derived from the literature.[34]

Connections Between the Beds. The volume of the connections between the vessels in Figure 1 is assumed to be negligible. Moreover, no discussion is reported about how the heat is removed or provided to the solids while they are

recirculated through these connections. Nevertheless, the solids are assumed to be fed to each vessel at the same temperature at which the vessel operates, and the heat duties associated with these changes in the temperature of the solids are accounted for in the overall thermal duty of the process.

Computational approach

Simulation of the Operation of a Single Bed. Considering a system of N components, z is the only independent variable for the mass and energy balances.

As regards the mass balance, N equations 1 for the whole bed and $N+1$ differential equations 2 are solved to determine the value of $2N+1$ dependent variables, i.e., N average solid loadings, $\bar{n}_i$, N gas phase concentrations, C_i, and the superficial velocity of the gas, u.

As for the energy balance, Eqs. 11 and 12 are solved to determine the values of the heat duty $\dot{Q}$ and of the required heat exchange surface p_{exch}, whereas one differential equation, either Eq. 17 or Eq. 18, is solved to determine the value of one dependent variable, which describes the properties of the external heat exchanging fluid, T_{fluid} or x_{v}, respectively.

According to the assumption of isothermal operation of the reactor at given temperature T, the energy balance can be solved separately once the mass balance has been solved. Given the nonlinear nature of the equations involved, numerical iterative processes are employed to solve the system of equations. For both the mass and the energy balances, in order to couple global and local systems of equations, internal iteration loops for the local balances are inserted into an external iteration loop for the global balance. All equations are implemented into a MATLAB script, and MATLAB built-in numerical solvers are employed to solve the systems of equations.

Simulation of the Separation Process. The simulation of the single riser is repeated for each vessel in the given configuration. If the riser is an adsorber, the inlet gas properties are known and the operation can be directly simulated. If the riser is a regenerator, instead, an additional iterative process is needed, because a fraction of the outlet stream (which is a priori unknown) is used as inlet gas to fluidize the bed. A MATLAB built-in numerical solver is used to compute the composition of this stream.

Circulating fluidized bed processes operate at steady state. The initial loading of the regenerated sorbent fed at riser inlet depends on the output of the regeneration process; likewise, the loading of solids at regenerator inlet will be defined by the output of the adsorber (Figure 1). In computational terms, an iterative process is needed to find the steady state conditions under which solids alternatively undergo adsorption and regeneration, being loaded and unloaded always to the same extent. Similarly to what is done for fixed bed simulations,[35] the simulation of the process starts considering that fresh sorbent is fed to the adsorption section. Then the adsorption and the regeneration sections are simulated in series, tracking the path a single solid particle would follow in the system, until the conditions for the steady state operation are reached. In the model, the mathematical condition for convergence to the steady state is identified by the following quantities, which must be lower than an assigned tolerance ζ_{tol}, set at 10^{-5}:

1. Solid loading: the maximum relative difference in the loading of the sorbent, $n_{i,j}$, for each i-th adsorbed compound at the outlet of every j-th reactor between two consecutive simulations (k and $k+1$), computed as

$$\Psi_1^{k+1} = \max_{i,j} \left\{ \left| \frac{2\,(n_{i,j}^{k+1} - n_{i,j}^{k})}{n_{i,j}^{k+1} + n_{i,j}^{k}} \right| \right\} < \zeta_{\text{tol}} \tag{19}$$

2. Gas composition: the maximum relative difference in the molar fractions in the gas phase, $y_{i,j}$, for each i-th compound at the outlet of every j-th reactor between two simulations (k and $k+1$), computed as

$$\Psi_2^{k+1} = \max_{i,j} \left\{ \left| \frac{2\,(y_{i,j}^{k+1} - y_{i,j}^{k})}{y_{i,j}^{k+1} + y_{i,j}^{k}} \right| \right\} < \zeta_{\text{tol}} \tag{20}$$

3. Gas flow rate: the maximum relative difference in the mass flow rate of the gas stream, $\dot{m}_j$, at the outlet of every j-th reactor between two simulations (k and $k+1$), computed as

$$\Psi_3^{k+1} = \max_{j} \left\{ \left| \frac{2\,(\dot{m}_j^{k+1} - \dot{m}_j^{k})}{\dot{m}_j^{k+1} + \dot{m}_j^{k}} \right| \right\} < \zeta_{\text{tol}} \tag{21}$$

4. Material balance: the maximum relative error obtained by computing the single-component material balance over the whole system for each i-th compound, as follows

$$\Psi_4^{k+1} = \max_{i} \left\{ \frac{F_i^{\text{feed}} - F_i^{\text{stack}} - F_i^{\text{capt}}}{F_i^{\text{feed}}} \right\} < \zeta_{\text{tol}} \tag{22}$$

where the molar flow rates, F, are named "feed" to indicate the flue gas at the inlet of the separation process, and "stack" and "capt" to indicate the streams leaving the adsorption section and the regeneration section, respectively.

The final error associated to the simulation of a single vessel is calculated as the maximum among all the values above.

Input data

The input dataset needed to simulate the operation of the system consists of four main subsets:

1. Sorbent data, which comprise information about the isotherm shape and the particle geometry (Table 1). Particle size has to be limited to a few hundreds micrometers, in order for the solids to be transported by the gas flow. In particular, the particle size chosen here belongs to the so-called B group of Geldart's classification[36]; this corresponds to aeratable noncohesive particles with a solid density ρ_{s} lower than 1.4 g/cm^3 and an average equivalent diameter smaller than 500 μm. For the purpose of this study, a common commercially available solid sorbent is considered, namely Zeolite 13X, pelletized into spherical particles of the size suitable for CFB applications.

2. Flue gas properties. The considered composition and flow rate are representative of a typical coal-fired supercritical boiler flue gas[38] after desulphurization (and translating the fraction of residual oxygen into nitrogen). The flue gas is assumed to be initially saturated in water. Therefore, it is treated in a drying unit before entering the capture unit. In fact, pre-drying of the gas mixture is necessary to avoid water adsorption on the solid, which is detrimental for most commercial sorbents (e.g., CO_2 capacity reduction, hysteresis between regeneration and adsorption). The energy required for the drying of the gas stream, which is assumed to be saturated in water, is taken into account when computing the overall energy consumption for CO_2 capture. The drying process performed with adsorption on silica gel is accredited with an energetic consumption of 8 MJ per kg of water removed from the flue gas.[39] At the inlet, a dry binary mixture of N_2 and CO_2 is fed. The properties of the flue gas stream are listed in Table 2.

Table 1. Sorbent Data, According to Hefti et al.[37]

Sorbent		
Material	Zeolite 13X	
Particle shape	Spherical	
Particle diameter, d_p [μm]	200	
Particle density, ρ_s $\left[\frac{kg}{m^3}\right]$	1085	
Specific heat capacity, c_s $\left[\frac{J}{kgK}\right]$	920	
Thermal conductivity, k_s $\left[\frac{W}{mK}\right]$	0.2	

Expressions for Sips isotherm coefficients:

Saturation capacity, $n_i^{\infty}=A_i^{\infty}\exp\left(-\frac{B_i^{\infty}}{RT}\right)$

Affinity coefficient, $\kappa_i=A_i^{\kappa}\exp\left(-\frac{B_i^{\kappa}}{RT}\right)$

Surface inhomogen. param.,
$\gamma_i=A_i^{\gamma}\,\mathrm{atan}\left(B_i^{\gamma}\left(T-T_i^{ref}\right)\right)+\gamma_i^{ref}$, $0<\gamma_i\leq 1$

Sips isotherm coefficients	CO_2	N_2
A_i^{∞} $\left[\frac{mol}{kg}\right]$	3.77	2.06
B_i^{∞} $\left[\frac{J}{mol}\right]$	−1802.3	−1701.4
A_i^{κ} $\left[\frac{L}{mol}\right]$	4.44×10^{-3}	10.04×10^{-3}
B_i^{κ} $\left[\frac{kJ}{mol}\right]$	−27.158	−13.642
A_i^{γ} [−]	528.73×10^{-3}	0
B_i^{γ} [−]	4.996×10^{-3}	0
γ_i^{ref} [−]	0.337	0.987
T_i^{ref} [K]	298.15	0
Heat of adsorption, Δh_i^{ads} $\left[\frac{kJ}{mol}\right]$	−34.20	−15.97
Lumped mass transfer coefficient, ω_i $\left[\frac{1}{s}\right]$	0.15	1.00

Table 2. Flue Gas Data, Bed Design Data, and Operating Conditions

Flue gas			
Composition	CO_2	N_2	H_2O
y_i (before drying) [% in moles]	14.56	81.20	4.24
y_i (after drying) [% in moles]	15.20	84.80	0
Inlet temperature, T_{feed} [°C]		30	
Inlet pressure, p [bar]		1.1	
Inlet flow rate, $\dot{m}_{feed}$ $\left[\frac{kg}{s}\right]$		781	
Bed design			
Inlet superficial velocity first ADS, u_{inlet} $\left[\frac{m}{s}\right]$		3	
Inlet superficial velocity each REG, u_{inlet} $\left[\frac{m}{s}\right]$		3	
Total cumulative height, H_t^{tot} [m]		15	
Dense zone solid volumetric fraction, ε_s^d [−]		0.16	
Lean zone asymptotic solid vol. fr., ε_s^{asym} [−]		0.02	
Constant product Λu^{inlet} $\left[\frac{1}{s}\right]$		8	
Heat trans. coeff. constant, γ_h		0.25	
Operating conditions			
Adsorption temperature, T_{ADS} [°C]		30	
Regeneration temperature, T_{REG} [°C]		Varied parameter	
Reactor pressure, p [bar]		1.1	
Sorbent flow rate, G_R $\left[\frac{kg}{m^2 s}\right]$		Varied parameter	
Solid inventory, W_s $\left[\frac{kg}{m^2}\right]$		Varied parameter	

Table 3. External Heating and Cooling System Data

External cooling system	
Walltube diameter, d_{WT} [m]	0.035
Fluid	Liquid water
Inlet temperature, T_w^{inlet} [°C]	15
Pressure, p_w [bar]	1
Max. velocity, u_w $\left[\frac{m}{s}\right]$	3
Density, ρ_w $\left[\frac{kg}{m^3}\right]$	998.0
Specific heat capacity, c_w $\left[\frac{J}{kgK}\right]$	4180
Thermal conductivity, k_w $\left[\frac{W}{mK}\right]$	0.6
Dynamic viscosity, μ_w $\left[\frac{kg}{ms}\right]$	0.0015
External heating system	
Walltube diameter, d_{WT} [m]	0.035
Fluid	Condensing steam
Inlet temperature, T_v [°C]	$T_{REG}+20$
Inlet vapor quality, x_v^{inlet} [−]	1
Max. inlet velocity, u_v^{inlet} $\left[\frac{m}{s}\right]$	15

3. Bed design: vessel sizes, inventories, reactor temperatures, and pressure levels are assigned. The superficial velocity is set as input value at the first vessel of the adsorption section and at each regenerator. The cross section area for the adsorption vessel is computed from the flue gas volumetric flow rate and the inlet superficial velocity; for the sake of simplicity, the same cross section is adopted in the regeneration vessel as well, so that the two sections operate with the same specific sorbent flow rate, G_R. The recirculated gas flow rate in the regenerators is set such to provide the desired superficial velocity at inlet, according to the input data. The total cumulative vessel height of both adsorption and regeneration section is fixed. In multiple-step configurations, this height is divided equally among the different vessels. The set value H_t^{tot} is chosen in such a way to obtain an aspect ratio H_t/L of at least 3 in most configurations and to be compatible with the height of the dense zone, according to the considered range of solid inventories. While pressure and adsorption temperature T_{ADS} are fixed in all simulations, solid inventories, W_s, recirculated sorbent flow rate, G_R, and regeneration temperature, T_{REG}, are varied to explore different operating conditions and process performance, as reported in Table 2.

4. External heating and cooling system data. All parameters used for heat transfer at riser walls are reported in Table 3. For the chosen values of these parameters, heat transfer at the exchanger surface is strongly limited by the heat resistance on the bed side, being this at least one order of magnitude higher than the heat resistance between the exchanging fluid and the tube wall (both for liquid water and steam). In fact, depending on the void fraction, on the gas composition and on the superficial velocity, the heat transfer coefficient ranges from around 30 W/m^2/K, for a very lean suspension, to around 1000 W/m^2/K, in the densest region. The range of flow rates for the external fluid are large enough to limit the temperature variation to a few degrees Celsius, in the case of liquid water, or to avoid complete condensation of the stream, in the case of vapor.

Performance indicators

In order to assess the separation performance of the system under investigation, two different indexes are considered in this work, namely recovery and purity, defined as:

$$\text{Recovery} = \frac{\dot{m}_{CO_2}^{capt}}{\dot{m}^{feed}\, x_{CO_2}^{feed}} = 1 - \frac{\dot{m}_{CO_2}^{stack}}{\dot{m}^{feed}\, x_{CO_2}^{feed}} \quad (23)$$

$$\text{Purity} = y_{CO_2}^{capt} \quad (24)$$

where the denomination "feed" indicates the flue gas at the inlet of the separation process, whereas "stack" and "capt" indicate the streams leaving the adsorption section and the regeneration section, respectively.

While the recovery affects the overall size of the plant, the purity is linked to the minimum requirements to be fulfilled for CO_2 transportation and storage. A "recovery–purity" diagram is widely employed in this work to display the performance of the system in terms of accomplishment of the separation specifications.

In order to consider the overall costs ascribed to the gas separation, including both the capital cost and the operational cost, two parameters are commonly employed. Both refer to the flow rate of CO_2 captured, $\dot{m}_{CO_2}^{capt}$, so as to be independent from the plant scale. The first one is productivity, computed as:

$$\text{Productivity} = \frac{\dot{m}_{CO_2}^{capt}}{(A_{ADS} + A_{REG})\, W_s} \quad (25)$$

where A_{ADS} and A_{REG} indicate the cross section areas for the adsorption and the regeneration sections, respectively. It is expressed in $kg_{CO_2}/(t_{ads}\, h)$ to indicate the necessary amount of sorbent, but it can also be translated into $kg_{CO_2}/(m^3\, h)$ to indicate the required vessel volume, which is closely related to the total size of the plant (hence to the CapEx).

The second index is the specific energy consumption, which is given by:

$$\text{Specific energy consumption} = \frac{\dot{Q}_{heat}}{\dot{m}_{CO_2}^{capt}} \quad (26)$$

where $\dot{Q}_{heat}$, in MW_{th}, is the sum of all the positive heat duties entering the system. These include not only the heat provided to regenerate the sorbent, but also the heat required for the drying of the flue gas. Thermal dispersions are neglected.

Beside assessing the requirements in terms of thermal energy, a more comprehensive index, the electrical equivalent consumption (in MJ_{el}/kg_{CO_2}), can also be defined. It considers the electrical equivalent of the provided heat, i.e., the amount of electric energy which would have been produced by the steam bled from the steam turbine (thus not expanded) to provide thermal power to the regenerator. Besides this, it also includes the heat rejected associated with the cooling duty (i.e., the electric consumption needed by a refrigerator to reject an equal amount of heat to the ambient) and the electrical consumption of the fans used to convey the gas streams through the vessels:

$$\text{Electrical equivalent consumption} = \frac{P_{el}}{\dot{m}_{CO_2}^{capt}} = \frac{P_{not\,exp}(T_{REG}) + P_{heat\,rej} + P_{fans}}{\dot{m}_{CO_2}^{capt}} \quad (27)$$

These two indices are representative of the OpEx of the plant.

A "specific energy consumption–productivity" diagram is used to represent the results obtained in terms of process performance.

Results

In order to assess the performance of the five configurations considered (standard configuration, two-step and three-step I-MS, two-step and three-step CTR-MS), a parametric analysis has been carried out where three design variables have been extensively varied:

- the temperature in the regeneration step, T_{REG};
- the mass flow rate of solid sorbent fed into each reactor (per unitary cross section area), G_R;
- the total solid inventory of the adsorption section (per unitary cross section area), W_s, which is always equal to the solid inventory of the regeneration section.

Table 4. Range of Values for the Three Parameters Varied in this Work

Parameter		Values
T_{REG}	[°C]	125, 150, 175, 200, 225, 250, 275, 300
G_R	$\left[\frac{kg_s}{m^2\, s}\right]$	From 0.4 to 30
W_s	$\left[\frac{kg}{m^2}\right]$	350, 500, 650, 800, 950, 1100, 1250, 1400

Table 4 shows the selected ranges of values for those input variables. Overall, more than 15,600 simulations have been performed.

In the following, results are reported in terms of: separation performance (recovery–purity), energy requirements, and productivity.

Among the different conditions investigated, some cases cannot reach a feasible steady state condition, thus the simulation could not converge. In particular, there exist input conditions for which the average loading of the solids is higher in the regenerator than in the adsorber. This might happen with an isolated multistep configuration when, for instance, a large amount of solids is circulating and most of the carbon dioxide is adsorbed within the first reactor. In the following reactors, the difference in CO_2 concentration between regeneration and adsorption might overcome the difference in temperature, leading to a solid enrichment in CO_2 within the regenerator, which eliminates the possibility of partially recirculating the gas to fluidize the bed. The results presented here include only those cases in which simulations have converged within the specified tolerances.

Separation performance

Figure 5a shows the performance of all the simulated operating points on a recovery–purity diagram. Points spread from the low-recovery/high-purity corner to the high-recovery/low-purity corner, showing that a clear trade-off between the recovery and purity exists. Notably, none of the simulated conditions managed to reach very high purity (>99%), and only a few points fulfill the specifications required for storage purposes (i.e., 90% recovery and 95% purity). Recovery rates span instead the whole range of possible values.

The figure also shows the Pareto frontiers for the different configurations. Both isolated and counter-current configurations outperform the basic configuration, with the counter-current one being able to provide both higher recovery rates and higher purities. The advantage of the counter-current multistep (CTR-MS) configuration stems from the better usage of the sorbent capacity for CO_2 adsorption. In fact, as the fresh regenerated sorbent is first fed into the lowest-CO_2-concentration reactor, a strong driving force allows to adsorb the last CO_2 left in the flow gas, together with a certain amount of N_2. As the solids proceed countercurrently through the adsorber

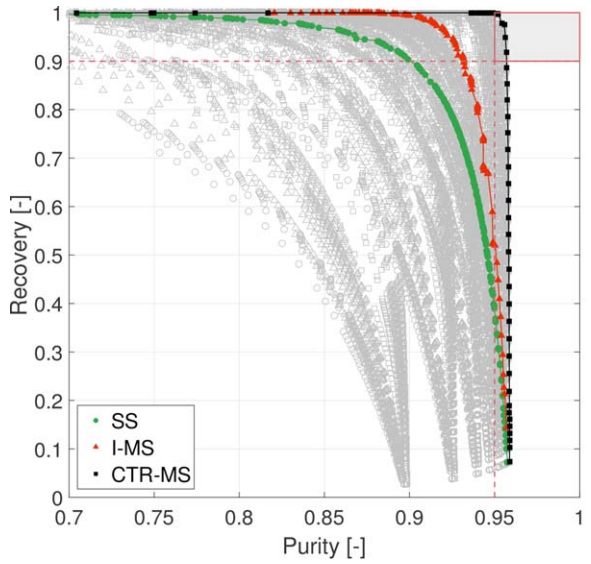

(a)

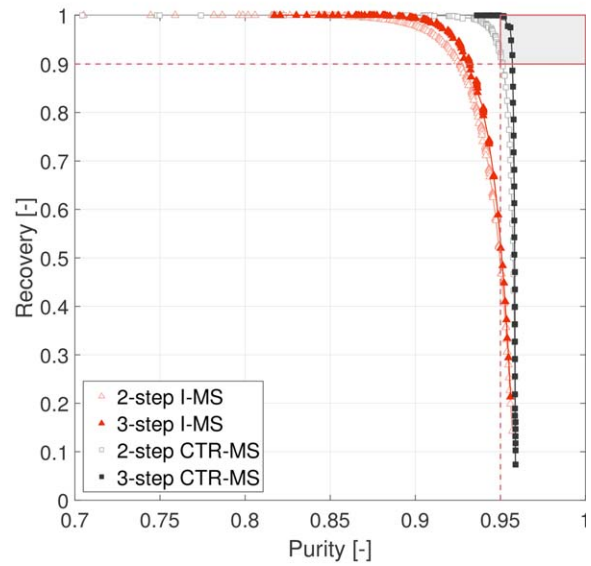

(b)

Figure 5. Recovery–purity diagram: Pareto fronts depending on (a) the configuration and (b) the number of steps.

[Color figure can be viewed at wileyonlinelibrary.com.]

series, most N_2 is displaced from the sorbent surface in favor of CO_2, thus preventing any purity decay.

The advantage of increasing the number of steps is illustrated in Figure 5b: for both isolated multistep and CTR-MS cases, the performance enhancement is noticeable when going from the two-step to the three-step design.

Figure 6 shows how the operating parameters affect the separation performance: results are reported only for the CTR-MS configurations; the same trends are observed for all the other configurations.

Both maximum purity and recovery are strongly affected by the regeneration temperature, T_{REG}, (Figure 6a). A T_{REG} value of 200°C is sufficient to reach recovery rates over 99.5%, while the purity does not exceed 96% for any of the tested regeneration temperatures. Moreover, given the trade-off between recovery and purity, the points that are characterized by the highest purities inevitably lie in the region of low recoveries. Higher temperatures correspond to lower loadings at equilibrium. Thus, increasing T_{REG} allows for deeper regeneration of the solid sorbent and consequently enhances recovery rates. The maximum reachable purity is instead closely connected to the shape of the binary CO_2/N_2 isotherm. Since the regenerator is fluidized with recycled CO_2-product, the gas phase composition is directly proportional to the amount of CO_2 and N_2 that are desorbed from the solids, i.e., to the cyclic capacity for each species. Therefore, to reach the desired purity specification, the cyclic capacity for CO_2 has to account for 95% of the sum of the two cyclic capacities. It can be demonstrated that, according to the binary isotherm and assuming to reach equilibrium at feed concentration in the adsorber and at product concentration in the regenerator, this condition can be reached for a minimum T_{REG} slightly over 190°C; for higher temperatures, the capacity for CO_2 accounts for a higher fraction of the sum, because the CO_2 isotherm is in absolute terms more sensitive to a temperature variation than the N_2 isotherm, and purity increases. Given the finite residence time of solids and an average concentration of CO_2 in the adsorber lower than the feed one, it can be foreseen that temperatures even higher than 190°C are required in the process to meet the purity specification; this is in fact only possible for a T_{REG} of at least 225°C, as shown in Figure 6a. Moreover, the performance is indeed enhanced for higher T_{REG} values, but the marginal benefit is progressively reduced as T_{REG} is increased, consistently with the fact that the isotherm gets progressively less sensitive to a variation of temperature.

The average residence time of particles in the reactors plays a key role in the overall separation performance of the process. It is given by the ratio between W_s and G_R. As indicated in Table 4, in this work the chosen ratio between the largest and the smallest value of W_s is 4, while the ratio between the highest and the lowest value of G_R is 75. Since the recovery is highly dependent on the average residence time of the particles, the broadness of the distribution of the operational points in the recovery–purity diagram has to be ascribed more to the variation of G_s than to that of W_s. Figure 6b shows the points colored according to G_R value. For larger solid flow rates, higher recovery rates and lower purities are obtained. The former are mainly due to the availability of sorbent material, which compensates the reduction of cyclic capacity caused by shorter residence times; the latter are due to the faster kinetics of adsorption of nitrogen compared to carbon dioxide, which penalize the CO_2/N_2 loading ratio for lower residence times.

As regards solid inventory, within the considered range of W_s the gas flow rates entrain always sufficient amounts of solids, i.e., $G_s \geq G_R$ according to Eq. 10 for each adsorber and each regenerator in every simulation. Figure 6c shows how the separation performance is affected by an inventory change. The effect on purity rates varies depending mostly on the cyclic capacity for CO_2. Purity is, in fact, directly proportional to the ratio between the cyclic capacities for the two components. The variation in N_2 loading due to the change of average time is however always much smaller, in absolute terms, compared to that of CO_2, because the equilibrium loading is lower and because adsorption kinetics for N_2 are faster ($\omega_{N_2} > \omega_{CO_2}$). For very low G_R values, when close to equilibrium conditions are reached in every vessel and the cyclic

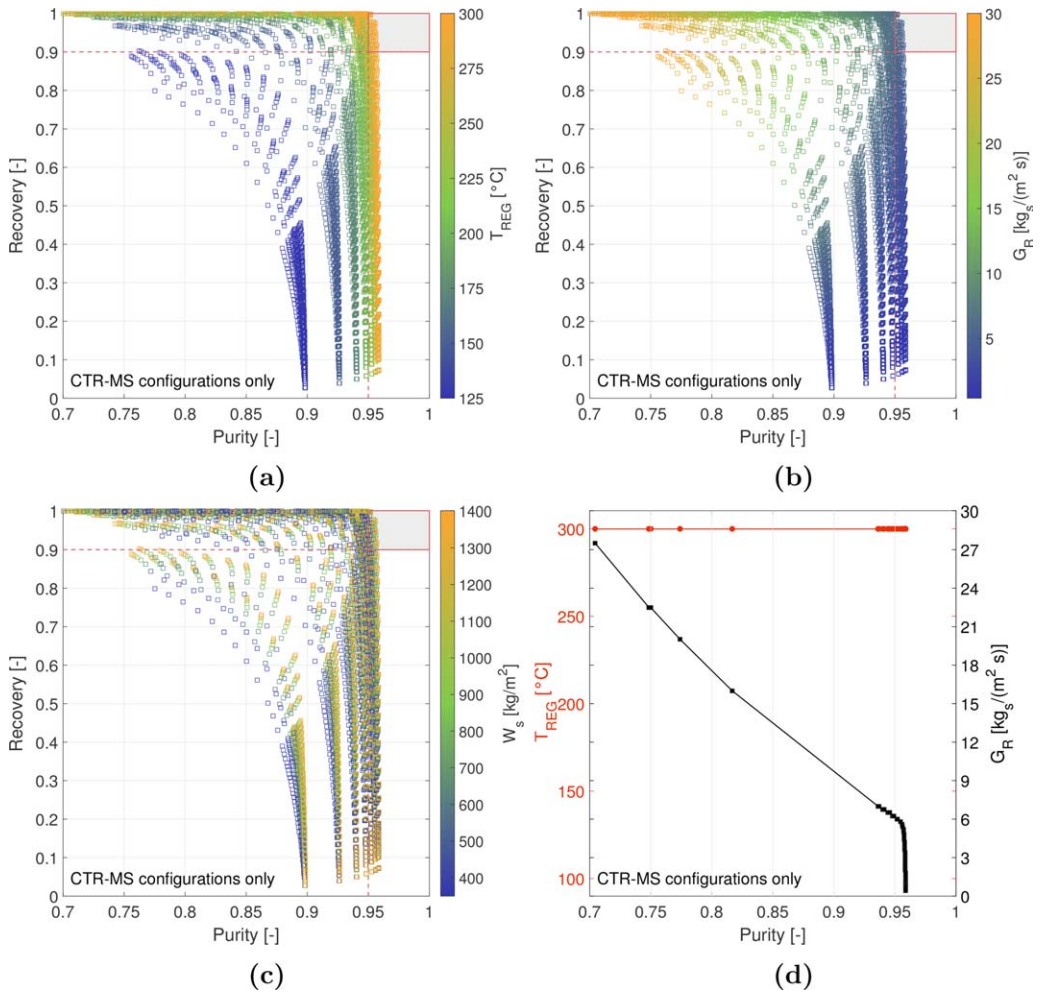

Figure 6. Recovery–purity diagram: dependence on the sensitivity analysis parameter (a) T_{REG}, (b) G_R, (c) W_s.

In (d) the variation of the most affecting parameters along the Pareto front for CTR-MS configurations of Figure 5a is shown. Only CTR-MS points are displayed. [Color figure can be viewed at wileyonlinelibrary.com.]

capacity for CO_2 is higher, a larger amount of N_2 adsorbed does not impact significantly on the final purity of the product; for very high G_R, instead, the same variation penalizes purity more. Therefore, increasing W_s compromises purity at high G_R, while it is mostly beneficial at low G_R.

Few differences can be noticed among the different configurations. The recovery rates for the two-step and three-step I-MS configurations appear to be much more sensitive to G_R, so that the highest recovery can already be reached with lower sorbent flow rates. At the same operating conditions, they feature higher recovery rates and lower purities, compared to the CTR-MS cases. The second and third adsorber are particularly efficient in capturing the CO_2 left at the end of the first step, despite the low concentration in the gas phase, which also promotes the adsorption of N_2. This causes N_2 concentration in the gas phase to be higher in the regenerator, thus the cyclic capacity increases (hence recovery is enhanced), whereas purity decreases.

Efficiency

In Figure 7a operating points that reach a recovery–purity performance of at least 90–95% are displayed in the productivity–energy consumption plane (both specific to the amount of captured CO_2) are shown, along with the resulting Pareto fronts for the different configurations. It can be observed that the low end energy consumption range starts at approximately 3.3 MJ/kg$_{CO_2}$.

As for the recovery–purity, the reactor configuration affects the energy–productivity results. None of the simulated single-step configurations reached the separation specifications. As regards the multi-step configurations, instead, the specifications are achieved only with CTR-MS systems. If the productivity of the multi-step cases is compared with that of the single-step one, at fixed operating conditions, better efficiency is found for the two-step and three-step configurations, both isolated and counter-current, thanks to the higher recovery rates.

The energy need is strongly affected by the different handling of the recirculated solids. While in the I-MS configurations every adsorber–desorber block has a dedicated solid loop, in CTR-MS there is only one loop. This implies that, in CTR-MS configurations, there is only one stream of solids that is heated up to the regeneration temperature, while in the isolated case there are as many as the number of blocks, each of them featuring a flow rate equal to G_R. Nevertheless, given the fact that recovery rates increase with G_R at a higher rate for I-MS configurations, to obtain the same performances less solids must be heated compared to CTR-MS systems, resulting in comparable energy consumptions for the two cases.

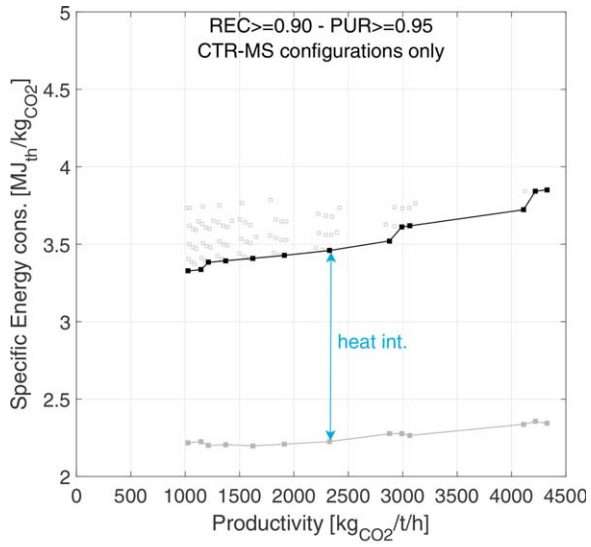

(a)

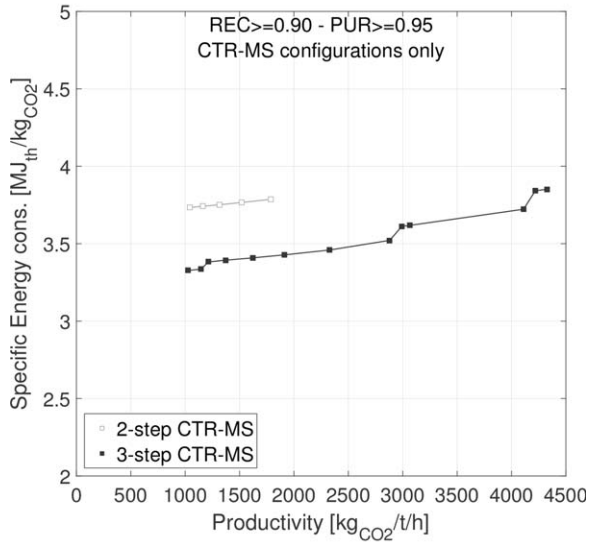

(b)

Figure 7. Energy consumption–productivity diagram: Pareto fronts for CTR-MS configuration (a) with and without heat integration and (b) depending on the number of steps.

In (a), for the points forming the Pareto front, the specific energy consumption has been re-computed after considering a 70% recovery of the sensible heat stored in the solids after regeneration, as explained in the discussion of the efficiency results. Only points meeting 90–95% recovery–purity specifications are displayed. [Color figure can be viewed at wileyonlinelibrary.com.]

Figure 8a shows the effect of T_{REG} on the energy–productivity results. Moving toward higher regeneration temperatures yields higher recoveries, which are directly translated into higher productivities. The effect on the specific energy consumption is instead twofold: The request for larger amounts of heat is always at least partially counteracted by the overall enhancement of recovery, so that an increase in T_{REG} is not unequivocally conducive to larger specific energy consumption (see Figure 8a). On the other hand, the influence of this parameter on the productivity is marginal.

To better understand the trend in the energy consumption, G_R has to be considered (Figure 8b). A considerable fraction of the heat provided to the system is used to heat up the solids that are conveyed from the adsorption to the regeneration section. The sensible heat stored in these solids depends on both G_R and T_{REG} (for a fixed adsorption temperature). The lowest energy consumption is reached when G_R is large enough to provide high recovery, yet limiting the heat required by the solids. For these reasons there is an optimal G_R value that minimizes the energy consumption.

W_s, within the range of investigated values, does not affect significantly the results in terms of energy consumption. Larger inventories imply slightly lower energy consumptions, as the recovery increases along with the average residence time, while no additional heat is needed. As regard productivities though, they yield worse performance (if mass-specific productivities are considered), proving how the disadvantage of increasing the inventory overcomes the recovery benefit (Figure 8c).

The specific energy consumption is a function of the overall heat power provided to the system. This heat power consists of two terms: on the one hand, the amount of heat directly provided to operate the regeneration vessel isothermally, as the endothermic desorption process would otherwise decrease the temperature of the bed; on the other hand, the amount of heat required to heat up the fully loaded solids from the adsorption temperature to the regeneration one. The latter term accounts for 65–95% of the total heat needed by the separation process (i.e., excluding drying), and is directly dependent on the G_R, on the process configuration and on the difference in temperature between the adsorption and the regeneration section. This heat is assumed to be provided to the solids before their entrance in the regenerator, namely in a separated fluidized bed heat exchanger so as to reduce the heat transfer surface required in the reactor. In a more complex configuration, a large part of the sensible heat could be recovered from the cooling of the solids traveling in the opposite direction (i.e., from regenerator to adsorber), for example by means of an interposed heat transfer loop. The benefit which can be reached by recovering 70% of this sensible heat is shown in Figure 7a, where the reduced energy consumption value is indicated for the points belonging to the Pareto front.

As regards the first term, instead, calculations have been performed in order to evaluate the feasibility of the heat exchange through the reactor walls, taking into account both the heating and the cooling of the vessels.

Through the definition of the length L, the geometry of the vessel can be adjusted to exchange the heat duties required for isothermal operation. However, as regards the aspect ratio H_t/L of each inner compartment, a minimum value of 3 has been assumed to guarantee an homogeneous distribution of the gas flow across the vessel; on the other hand, a minimum distance between two parallel heat exchanging walls (i.e., the compartment depth, L) of at least 20 cm is here considered as lower feasibility limit for realization purposes. In Figure 8d the red points represent those operating conditions, for which the isothermal operation of the vessels is compatible with this geometry specifications. It can be immediately observed that many points cannot be operated while satisfying at the same time these conditions, and additional heat transfer surface (e.g., additional heat transfer panels inside the riser, external fluidized bed heat exchanger, increased gas recycle to increase reactor volume) would be needed to guarantee isothermal

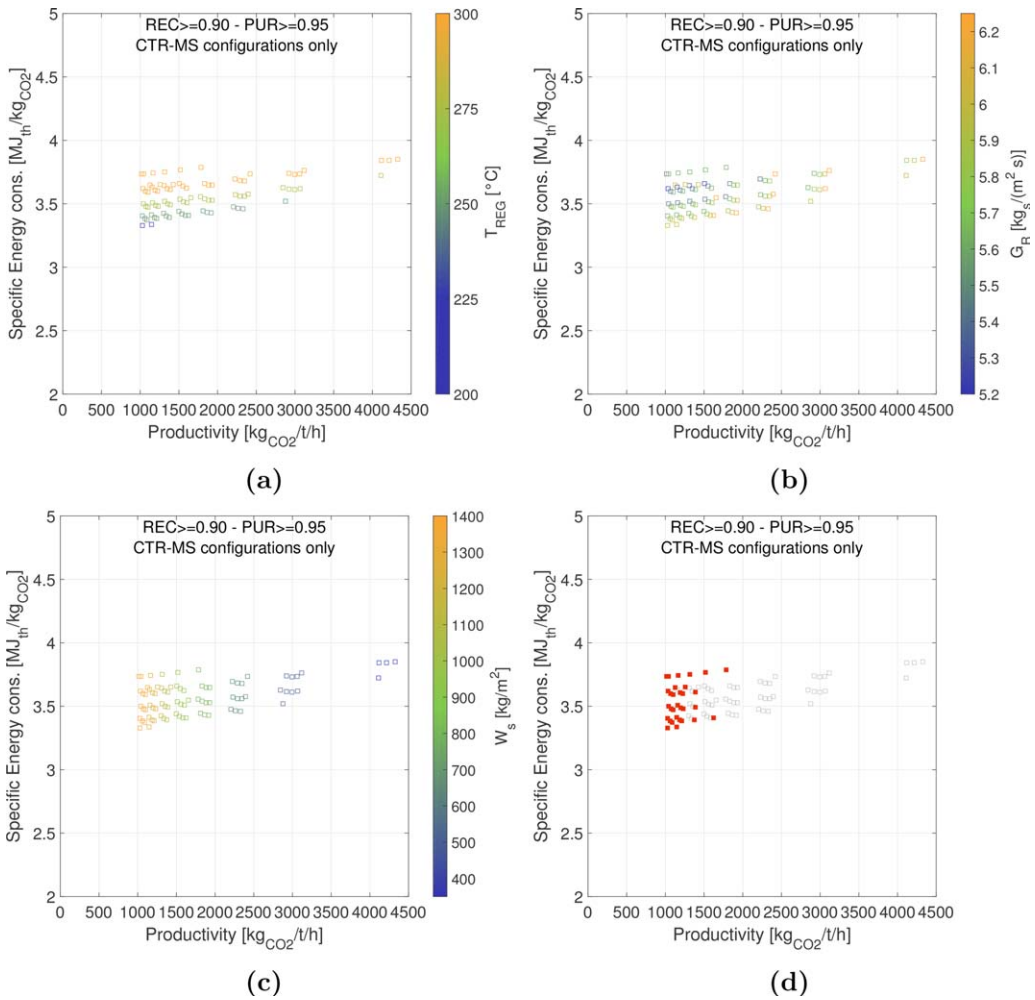

Figure 8. Energy consumption–productivity diagram: dependence on the sensitivity analysis parameter (a) T_{REG}, (b) G_R, (c) W_s.

In (d) the points having a minimum H_t/L aspect ratio of 3 and minimum distance between walls of 20 cm are highlighted in red. Only CTR-MS points meeting 90–95% recovery–purity specifications are displayed. [Color figure can be viewed at wileyonlinelibrary.com.]

operation at the given temperature. The surface area needed to exchange all the heat associated with the adsorption process is related not only to to the amount of heat to be exchanged, but also to the heat resistance from the bed to the external thermovector fluid. As a consequence, two effects should be accounted for:

- For higher G_R levels recovery is enhanced, which means more mass is transferred between gas and solid phase, and more heat has to be either released by or provided to the bed. Therefore larger surface is needed, which corresponds to higher aspect ratios;
- For higher W_s values the average solid volume fraction within the vessel ε_s is larger, as H_d increases with the inventory (Eqs. 6 and 7). Since higher solid density significantly enhances the heat transfer between the suspension and the reactor walls (Eqs. 13 and 14), the needed surface is reduced for larger specific inventories (which also correspond to lower purities).

The same operational points displayed in Figure 8d are illustrated in Figure 9, this time considering the electrical equivalent of their specific energy consumption. Operating conditions, performance and vessel geometry of the best performing conditions are summarized in Tables 5 and 6.

As regards the relevance of the different terms forming the electrical equivalent energy consumption, the term related to the steam that is not expanded is in most cases predominant, accounting for at least 90% for any point which features a recovery larger than or equal to 50%. The term associated with the heat rejection of the cooling system follows the same trends as the previous one, but it is approximately 50 times smaller. The term related to the electrical consumption of the fans is directly proportional to the solid inventory and sums up to less than 0.1 MJ/kg_{CO_2} for any point with recovery $\geq$30%.

From the analysis of these results, it can be observed that the heat exchange at the tubewalls is critical to the operation of the system, both in the adsorbers and in the regenerators. In order to transfer the heat in and out of the fluidized beds, very large exchanging surfaces are needed.

None of the highlighted operating points features a small solid inventory value. In fact, because of the effects mentioned above, small inventories and high recovery rates are incompatible. Moreover, as the regeneration temperature increases, larger exchange surfaces are required, since this allows for higher recoveries. Among the adsorbers, the vessel where the solids are fed immediately after regeneration is the one where most of the CO_2 adsorbs and therefore the vessel where the

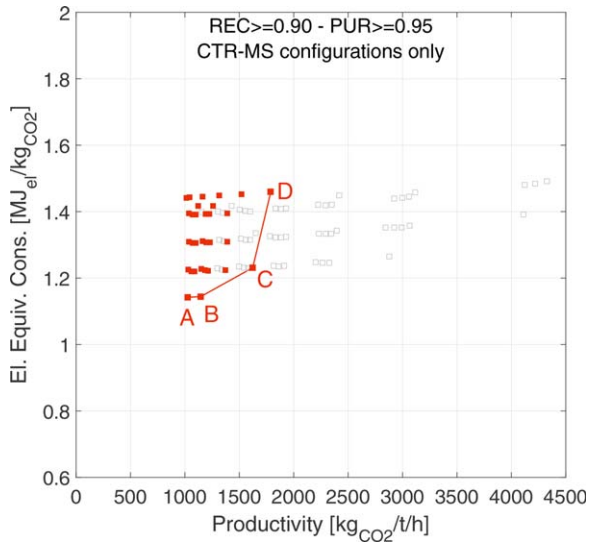

Figure 9. Electrical equivalent consumption–productivity diagram: heat exchange limitations.

Only points meeting 90–95% recovery–purity specifications are displayed. The points highlighted in red have a minimum H_t/L aspect ratio of 3 and minimum distance between walls of 20 cm. [Color figure can be viewed at wileyonlinelibrary.com.]

heat duty to be removed is larger. Limit values of the varied parameters can be identified in order to fulfill the limitations imposed on the vessel geometry. While for isolated multistep configurations (I-MS) and for the basic single-step configuration the correlation between these limit values of G_R and W_s is found to be rather linear, for CTR-MS configurations a much higher margin exists for larger inventory values. This effect is to be ascribed to the fact that the adsorption section is more limiting than the regeneration one, from a heat transfer point of view, due to the low ΔT between adsorber temperature and cooling water. Therefore the CTR-MS configurations can take advantage of the fact that adsorption is more evenly distributed among the different adsorption steps than in the isolated multistep configuration, where the first adsorber sees a steep decrease in CO_2 concentration, while the following ones are responsible for a smaller fraction of the overall recovery. Therefore, CTR-MS configurations are also less limited in terms of heat exchange.

Comparative assessment of the performance

The results of the TSA CFB system are compared with classical fixed bed TSA, amine-based scrubbing technologies and Ca-looping capture processes. The results, in terms of electrical equivalent of the thermal energy duty (the other components of the total electrical equivalent are in this case neglected) and productivity are illustrated in Figure 10. The performances of the amine process are given for a representative range of MEA[40]; those of the fixed bed TSA are taken from Joss et al.[13]; the data for the calcium looping process are derived from the work of Martínez et al.[41] and Romano.[42] The comparison is based on solutions that reach 90–95% recovery–purity, and therefore only the CTR-MS configuration is considered.

It can be noted that the electrical equivalent of the energy consumption, when solids do not exchange heat between adsorption and regeneration, is slightly larger than the state-of-the-art solutions and not far from that of fixed bed TSA. Fixed-bed TSA processes and absorption processes can be performed providing heat to the system at around 150°C. To reach the same recovery–purity specifications, a regeneration temperature of at least 225°C is instead required for CFB systems, due to the limitations associated with the adsorption equilibria mentioned above. The effect of these limitations is connected both with the configuration of the process and with the properties of the sorbent material. As regards the former, the gas concentration within the regeneration section must be constant, to perform a continuous process, and uniform, to fluidize the bed with recycled CO_2-product; in fixed-bed TSA cycles, where the evolution of the CO_2 concentration during the regeneration step can be exploited to separate a pure product from a less pure recycled stream, regeneration can be effectively performed at lower temperatures. As regards the latter, since

Table 5. Operating Points in Figure 9: Process Performance

	#Step	T_{REG} [°C]	G_R $\left[\frac{kg_s}{kg_{feed}}\right]$	W_s $\left[\frac{kg}{m^2}\right]$	Recov. [%]	Purity [%]	En. cons. $\left[\frac{MJ_{th}}{kg_{CO_2}}\right]$	El. eq. $\left[\frac{MJ_{el}}{kg_{CO_2}}\right]$	Prod. $\left[\frac{kg_{CO_2}}{t\,h}\right]$
A	3	225	6.0	1400	91.15	95.01	3.33	1.14	1026.9
B	3	225	6.0	1250	90.81	95.00	3.34	1.14	1145.8
C	3	250	6.25	950	97.78	95.08	3.41	1.23	1623.3
D	2	300	5.6	800	90.76	95.03	3.79	1.46	1789.3

Table 6. Operating Points in Figure 9: Vessel Geometry for Each Reactor

	ADS1			ADS2			ADS3			REG		
	L [m]	H_t [m]	L_w [m]	L [m]	H_t [m]	L_w [m]	L [m]	H_t [m]	L_w [m]	L [m]	H_t [m]	L_w [m]
A	1.266	5	15.40	0.353	5	55.24	0.227	5	85.90	0.505	15	38.61
B	1.188	5	16.41	0.335	5	58.20	0.211	5	92.42	0.485	15	40.21
C	0.524	5	37.21	0.201	5	97.01	0.237	5	82.27	0.401	15	48.62
D	0.368	7.5	52.98	0.206	7.5	94.66				0.393	15	49.62

Values are expressed for a total flue gas flow rate of 781 kg/s. The total vessel volume of the plant is constant and equal to ca. 5850 m^3, which corresponds to a footprint of ca. 390 m^2 for a total height of 15 m. The footprint is equally divided into the adsorption and the regeneration section. The reactor width L_w is expressed as a single value, derived as the ratio between the vessel cross section area and the vessel depth equal to $10L$. For high values of L_w, more vessels in parallel can be used instead of a single vessel, in order to maintain a convenient aspect ratio between vessel width and vessel depth for construction purposes; in this case, L_w corresponds to the cumulative width of the vessels.

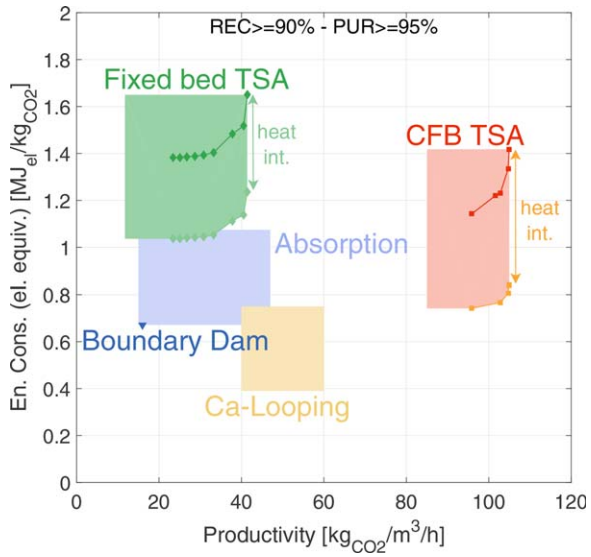

Figure 10. Energy consumption–productivity diagram: comparison with most established technologies in terms of electrical equivalent.

Only points meeting 90–95% recovery-purity specifications are displayed. According to Joss et al.,[13] energy consumption of fixed bed TSA systems can be reduced by means of heat integration, implementing temperature equalization between the cycle units and recovering heat from the hot flue gas. For CFB TSA systems, energy consumption can be reduced by means of heat integration, by recovering the sensible heat stored in the solids after regeneration, as explained in the discussion of the efficiency results. [Color figure can be viewed at wileyonlinelibrary.com.]

commercial CO_2 adsorbent, including Zeolite 13X, are highly selective toward water, they cannot be regenerated by means of a hot steam purge, which would allow reducing the concentration of CO_2 in the regenerator. However, if an alternative absorbent able to work in the presence of water were used, such steam purge could be used for regeneration, reducing in this way the regeneration temperature needed and thus the energy consumption.

For the calcium looping technology, the heat to regenerate the sorbent is provided to the solids at high temperature (usually between 600 and 950°C) by a direct combustion, which means that the residual heat can be easily used to run a steam power cycle. Most of the consumption, in terms of electrical duty, comes from the air separation unit that has to be installed to operate the oxy-combustion in the calciner.

For the CFB TSA, where heat integration between the two solid streams is possible, the energy consumption of the CFB systems could be significantly reduced. The sensible heat stored in the solids during the regeneration, as mentioned in the discussion of the efficiency results, accounts for the largest fraction of the total heat required by the system (from 50% to over 90%). For this reason, it can be reasonably assumed that around 20% of the overall thermal energy consumption could be cut by means of heat integration between streams of recirculated solids, as shown in Figure 10.

Concerning the productivity, the systems that rely on fast fluidized beds, i.e., both calcium looping and CFB TSA, significantly outperform the fixed-bed TSA and the amine scrubbing technologies, as it could be expected, given the higher spatial velocity of the gas. The further advantage of the TSA systems vs. the Ca-looping derives by the lower range of temperatures wherein the process is operated. The high temperatures reached in both the carbonator and the calciner of a Ca-looping application imply lower gas densities, which penalize the productivity on a volumetric base.

Conclusion

In this work, five different process configurations for post-combustion CO_2 capture via TSA with CFBs have been presented. All these configurations allow to operate the separation process continuously thus reducing the overall plant size as compared to standard fixed bed systems. In addition to the simple single step configuration, two different types of multiple step configurations have been proposed: an isolated multistep type, where solids and gas proceed in parallel through the series of adsorption steps; a counter-current multistep type, where solids and gas proceeds through the series of adsorption steps in opposite directions.

Stationary, isothermal operation of the reactors has been simulated by means of a model which couples a one-dimensional description of the CFBs with binary adsorption equilibria and adsorption kinetics. A commercial sorbent, i.e., pelletized Zeolite 13X, has been considered.

A sensitivity analysis has been performed over the five different process configurations, taking three different inputs as varying parameters: the regeneration temperature, the flow rate of solid sorbent fed to the reactors and the total solid inventory. Separation performance (recovery rate and product purity) and global efficiency (in terms of heat duty or electrical equivalent consumption vs. productivity) have been assessed for each feasible operating condition and the final results have been compared to the most established technologies for CO_2 separation.

The following conclusions can be drawn:

- Multi-step configurations outperform the simplest single-step process, both in terms of separation performance and in terms of global process efficiency. In order to reach the specifications imposed by a CCS application (90% recovery of the CO_2 in the flue gas, 95% purity of the captured CO_2), CTR-MS configurations must be employed, as neither the single-step nor the isolated multistep configuration reach those separation performance.
- Compared to both fixed-bed TSA processes and amine-scrubbing technologies, a significant reduction in plant footprint can be obtained by employing a CFB configuration, thus increasing the productivity (on a volumetric base) to levels even superior to those reached by calcium looping processes.
- While high recovery rates can be easily reached, purities are strongly limited by adsorption equilibria, so that only for high regeneration temperatures ($\geq$250°C) CO_2-purity values above 95% can be obtained. This significantly restricts the temperature range within which waste heat can be recovered to run the process.
- Specific energy consumption is lower, for given separation specifications, than that of fixed-bed TSA processes, but higher than that of the most established absorption-based technologies.
- In order to reduce the energy consumption, the sensible heat stored in the solids after regeneration should be recovered. To the author knowledge, no well-established technology is commercially available to exchange heat between two gas–solids suspensions at a reasonable efficiency rate.

• The handling of heat fluxes at vessel walls is also a major issue. Even assuming that the sensible heat stored in the recirculated solids is provided or recovered outside the vessels, the heat exchanging surface required at bed walls exceeds in most cases the actual maximum, as determined according to technical limitations. A different fluidization regime with lower gas velocities and longer residence times might be considered as an alternative option, although it would necessarily compromise the productivity performance.

Literature Cited

1. Boot-Handford ME, Abanades JC, Anthony EJ, Blunt MJ, Brandani S, Mac Dowell N, Fernandez JR, Ferrari MC, Gross R, Hallett JP, Haszeldine RS, Heptonstall P, Lyngfelt A, Makuch Z, Mangano E, Porter RTJ, Pourkashanian M, Rochelle GT, Shah N, Yao J, Fennell PS. Carbon capture and storage update. *Energy Environ Sci*. 2014;7:130–189. [TQ1]
2. Idem R, Supap T, Shi H, Gelowitz D, Ball M, Campbell C, Tontiwachwuthikul P. Practical experience in post-combustion CO_2 capture using reactive solvents in large pilot and demonstration plants. *Int J Greenh Gas Control*. 2015;40:6–25.
3. Office of Fossil Energy at National Energy Technology Laboratory. W.A. Parish Post-Combusion CO_2 Capture and Sequestration Project: Final Environmental Impact Statement (DOE/EIS-0473). U.S. Department of Energy (DOE), 2013.
4. Quest Carbon Capture and Storage Project: Annual Summary Report—Alberta Department of Energy: 2014. Shell Canada Ltd., 2015.
5. IEAGHG. Integrated Carbon Capture and Storage Project at SaskPower's Boundary Dam Power Station. IEA Environmental Projects Ltd., 2015.
6. Abanades JC, Arias B, Lyngfelt A, Mattisson T, Wiley DE, Li H, Ho MT, Mangano E, Brandani S. Emerging CO_2 capture systems. *Int J Greenh Gas Control*. 2015;40:126–166.
7. Webley PA. Adsorption technology for CO_2 separation and capture: a perspective. *Adsorption*. 2014;20(2–3):225–231.
8. Elseviers W, Flowers Hassett P, Navarre JL, Whysall M. *50 Years of PSA Technology for H2 Purification*. Des Plaines: Honeywell UOP LLC, 2015.
9. Merel J, Clausse M, Meunier F. Carbon dioxide capture by indirect thermal swing adsorption using 13X zeolite. *Environ Prog*. 2006;25:327–333.
10. Merel J, Clausse M, Meunier F. Experimental investigation of CO_2 post-combustion capture by indirect thermal swing adsorption using 13X and 5A zeolites. *Ind Eng Chem Res*. 2008;47:209–215.
11. Clausse M, Merel J, Meunier F. Numerical parametric study on CO_2 capture by indirect thermal swing adsorption. *Int J Greenh Gas Control*. 2011;5(5):1206–1213.
12. Ntiamoah A, Ling J, Xiao P, Webley PA, Zhai Y. CO_2 capture by temperature swing adsorption: use of hot CO_2-rich gas for regeneration. *Ind Eng Chem Res*. 2016;55:703–713.
13. Joss L, Gazzani M, Mazzotti M. Rational design of temperature swing adsorption cycles for post-combustion CO_2 capture. *Chem Eng Sci*. 2017;158:381–394.
14. Zhang W, Liu H, Sun C, Drage TC, Snape CE. Capturing CO_2 from ambient air using a polyethyleneimine-silica adsorbent in fluidized beds. *Chem Eng Sci*. 2014;116:306–316.
15. Yang WC, Hoffman J. Exploratory design study on reactor configurations for carbon dioxide capture from conventional power plants employing regenerable solid sorbents. *Ind Eng Chem Res*. 2009;48:341–351.
16. Ammendola P, Raganati F, Chirone R. CO_2 adsorption on a fine activated carbon in a sound assisted fluidized bed: thermodynamics and kinetics. *Chem Eng J*. 2017;322:302–313.
17. Girimonte R, Formisani B, Testa F. Adsorption of CO_2 on a confined fluidized bed of pelletized 13X zeolite. *Powder Technol*. 2017;311:9–17.
18. Yi CK, Jo SH, Seo Y, Lee JB, Ryu CK. Continuous operation of the potassium-based dry sorbent CO_2 capture process with two fluidized-bed reactors. *Int J Greenh Gas Control*. 2007;1:31–36.
19. Veneman R, Li Z, Hogendoorn J, Kersten S, Brilman D. Continuous CO_2 capture in a circulating fluidized bed using supported amine sorbents. *Chem Eng J*. 2012;207–208:18–26.
20. Kim K, Kim D, Park YK, Lee KS. A solid sorbent-based multi-stage fluidized bed process with inter-stage heat integration as an energy efficient carbon capture process. *Int J Greenh Gas Control*. 2014;26:135–146.
21. Pröll T, Schöny G, Sprachmann G, Hofbauer H. Introduction and evaluation of a double loop staged fluidized bed system for post-combustion CO_2 capture using solid sorbents in a continuous temperature swing adsorption process. *Chem Eng Sci*. 2016;141:166–174.
22. Zaabout A, Romano MC, Cloete S, Giuffrida A, Morud J, Chiesa P, Amini S. Thermodynamic assessment of the swing adsorption reactor cluster (SARC) concept for post-combustion CO_2 capture. *Int J Greenh Gas Control*. 2017;60:74–92.
23. Pirngruber GD, Guillou F, Gomez A, Clausse M. A theoretical analysis of the energy consumption of post-combustion CO_2 capture processes by temperature swing adsorption using solid sorbents. *Int J Greenh Gas Control*. 2013;14:74–83.
24. Jee JG, Kim MB, Lee CH. Adsorption characteristic of hydrogen mixtures in a layered bed: binary, ternary, and five-component mixtures. *Ind Eng Chem Res*. 2001;40:868–878.
25. Schell J, Casas N, Pini R, Mazzotti M. Pure and binary adsorption of CO_2, H_2 and N_2 on activated carbon. *Adsorption*. 2012;18(1):49–65.
26. Kunii D, Levenspiel O. *Fluidization Engineering*. Stoneham: Butterworth-Heinemann, Division of Reed Publishing Inc., 1991.
27. Haider A, Levenspiel O. Drag coefficient and terminal velocity of spherical and nonspherical particles. *Powder Technol*. 1989;58(1):63–70.
28. Chen JC. Heat transfer. In: Yang WC. *Handbook of Fluidization and Fluid-Particle Systems*. New York: Marcel Dekker Inc., 2003:252–281.
29. Lienhard IVJH, Lienhard VJH. *Heat Transfer*, 4th ed. Cambridge: Phlogiston Press, 2012.
30. Zhang HL, Baeyens J, Degrève J, Brems A, Dewil R. The convection heat transfer coefficient in a circulating fluidized bed (CFB). *Adv Powder Technol*. 2014;25(2):710–715.
31. Molodtsof Y, Muzyka DW. Wall to suspension heat transfer in the similar profile regime. *Int J Heat Mass Transf*. 1992;35(10):2665–2673.
32. Gnielinski V. Neue Gleichungen für den Wärme- und den Stoffübergang in turbulent durchströmten Rohren und Kanälen. *Forsch im Ingenieurwes*. 1975;41(1):8–16.
33. Dobson MK, Chato JC. Condensation in smooth horizontal tubes. *J Heat Transfer*. 1998;120:193–213.
34. Wagner W, Cooper JR, Dittmann A, Kijima J, Kretzschmar H-J, Kruse A, Mareš R, Oguchi K, Sato H, StöCker I, ŠIfner O, Takaishi Y, Tanishita I, TrüBenbach J, Willkommen T, The IAPWS industrial formulation 1997 for the thermodynamic properties of water and steam. *J Eng Gas Turbines Power*. 2000;122(1):150–184.
35. Casas N, Schell J, Joss L, Mazzotti M. A parametric study of a PSA process for pre-combustion CO_2 capture. *Sep Purif Technol*. 2013;104:183–192.
36. Geldart D. Types of gas fluidization. *Powder Technol*. 1973;7(5):285–292.
37. Hefti M, Marx D, Joss L, Mazzotti M. Adsorption equilibrium of binary mixtures of carbon dioxide and nitrogen on zeolites ZSM-5 and 13X. *Microporous Mesoporous Mater*. 2015;215:215–226.
38. European best practice guidelines for assessment of CO_2 capture technologies. CAESAR Consortium 2008–2011, 2011.
39. Bart HJ, von Gemmingen U. Adsorption. In: Bellussi G, Bohnet M, Bus J, Drauz K, Greim H, Jäckel KP, Karst U, Kleemann A, Kreysa G, Laird T, Meier W, Ottow E, Röper M, Scholtz J, Sundmacher K, Ulber R, Wietelmann U. eds. *Ullmann's Encyclopedia of Industrial Chemistry*. Weinheim: Wiley-VCH Verlag GmbH & Co. KGaA, 2012:549–620.
40. IEAGHG. Incorporating future technology improvements in existing CO_2 post combustion capture plants: Technical Review. IEA Environmental Projects Ltd., 2013.
41. Martínez I, Murillo R, Grasa G, Abanades JC. Integration of a Ca looping system for CO_2 capture in existing power plants. *AIChE J*. 2011;57(9):2599–2607.
42. Romano MC. Modeling the carbonator of a Ca-looping process for CO_2 capture from power plant flue gas. *Chem Eng Sci*. 2012;69(1):257–269.

Manuscript received Aug. 10, 2017, and revision received Oct. 19, 2017.